EIS as a Tool to Characterize Nanostructured Iron Fluoride Conversion Layers for Li-Ion Batteries

B. Guitián, X.R. Nóvoa, A. Pintos*

University of Vigo, ENCOMAT group, EEI, Campus Universitario, 36310 Vigo, Spain

In memory of Professor Zdravko Stoynov for his kind personality and innovative scientific contribution to electrochemistry

The present study aims at developing FeF_3 conversion layer on cheap mild steel substrates for use as cathode materials in Li-ion batteries. The coatings, grown in an ethylene glycol based electrolyte are characterised by SEM, FIB and EDX techniques that show the formation of similar porous structures but thicker for the mild steel substrate than for the iron substrate. The porous structure is characterised by EIS using a transmission line model that allows obtaining relevant parameters of the layer as the conductivity or the reactivity at pore walls. The conductivity of the FeF_3 layer is higher for the mild steel substrate than for the iron substrate. The FeF_3 layers react to some extent in LiBOB electrolyte which is interpreted as iron corrosion and Fe^{3+} reduction with Li^+ insertion in the FeF_3 structure.

Key words: Iron fluoride, Li-ion batteries, electronic conductivity.

INTRODUCTION

The Li-ion batteries sector is a major actor in the field of energy conversion and storage, mainly dealing with portable devices. The reaction mechanism in these batteries involves insertion reactions at both electrodes, the anode and the cathode. The cathode material and the electrical contact between active material and current collector continue to be the main limitations to increasing the capacity of Li-ion cells. An alternative strategy aimed at overcoming (at least partially) these drawbacks involves increasing the available charge and decreasing the internal ohmic resistance through the use of electrode materials directly grown on the current collector. Directly grown layers guarantee good electrical contact between the current collector and the active material. Moreover, if the electrode material is able to undergo conversion reactions, the nominal capacitance increases with respect to that of insertion reactions. Thus, the electrode material will reach all its entire range of oxidation states. Due to their high nominal capacity, transition metal fluorides, such as FeF_3 are good candidates for the conversion reactions with lithium ions [1,2].

Direct formation of a fluoride-based layer has been achieved by anodizing of iron strips in ethylene glycol and NH_4F as the electrolyte. Highly nanoporous layers of iron hydroxifluorides were obtained [3]. Nevertheless, those fluoride layers were of poor electronic conductivity, which limits their performance as electroactive materials.

One possible strategy to improve fluorides' conductivity is the incorporation of foreign conducting materials, such as carbon or conducting polymers[4]. The present work focuses on a different approach, according to which electronic conductivity improvements can be reached through the incorporation of conducting elements from inner sources. The idea is to synthesize active material as in [3], but using carbon steel as the substrate instead of pure iron. It is expected that the carbon dissolved in the alloy will accompany dissolving iron and will remain trapped in the matrix of fluorides, thus increasing its electronic conductivity. Electrochemical impedance spectroscopy (EIS) has been chosen as the tool to quantify the electronic conductivity of the porous layers formed, by modelling the electrochemical response obtained as a transmission line type distribution of the electric field.

EXPERIMENTAL

Preparation of the conversion coatings

The development of the conversion coatings was carried out by anodizing the substrate material in a two-electrodes cell as in [3]. The substrate material ran as a working electrode and a platinum mesh as

---

To whom all correspondence should be sent:
E-mail: apintos@uvigo.es

the counter electrode. The potential applied was 50V for 15 min and the electrolyte solution used was 0.1 M NH_4F in ethylene glycol containing water (3%). An Ivium® potentiostat (IviumStat.XRe) was employed for the anodizing procedure.

Two different materials were used as the substrate, iron strips as those employed in [3], and low carbon steel strips. The mild, with low carbon content steel, is expected to produce a conversion layer structurally close to that found for iron, although of higher electronic conductivity due to trapped carbon. Table 1 summarises the chemical composition of the main alloying elements.

Table 1. Main elements in the composition of the samples tested

		C	Fe
Mild steel	Atomic%	4.87	94.06
	Weight%	1.09	97.53
Iron		0.0	99.99

Morphological characterization of the conversion coatings

The morphological characterization of the films was done using Focused Ion Beam Scanning Electron Microscopy (FIB-SEM). The microscope was a Dual-Beam FEI Helios NanoLab. The SEM technique allowed us to gather information on the nanoporous morphology of the thin film, and the FIB technique was used to measure its thickness and to investigate the cross-section morphology.

Electrochemical characterization

The electrochemical characterization of the coatings obtained was performed through electrochemical impedance spectroscopy (EIS) and charge and discharge cycles. EIS measurements were performed using a Methrom-Autolab® potentiostat (PGSTAT 30). The EIS characterization was performed in two experiments:

a) Just after anodizing, with fresh electrolyte. In this case a three-electrode cell arrangement was employed, using a Pt mesh as a counter electrode, and a Pt wire as a pseudo–reference electrode.

b) Ageing in the typical electrolyte for Li-ion batteries. Lithium bis-oxalate-borate (LiBOB, 1M) + 2% fluoroethylene carbonate (FEC) dissolved in ethylene carbonate (EC) and dimethyl carbonate (DMC) (1:1 [v/v]) was chosen as electrolyte. Symmetrical cells were assembled in a pouch cell case inside a glove box with a dry atmosphere. We employed two

nominally identical electrodes, one acting as a working electrode and the other as a counter electrode. A film of glass fibre was used as a separator.

Cycling of the conversion coatings was also performed on pouch cell case arrangements, using the electrolyte described above. This electrolyte was chosen due to its good properties in the cycling of lithium ion batteries [5–7]. A lithium foil was employed as a counter electrode and a film of glass fibre as a separator. The cell was galvanostatically cycled applying 15 $\mu A \cdot cm^{-2}$ of current density in a potential window of 1 V - 4 V.

RESULTS AND DISCUSSION

Preparation of the conversion coatings

Figure 1 compares the chronoamperograms obtained for the Fe and steel anodizations. The general appearance is similar for both substrates. The three domains reported in [3] can be differentiated: germination, growth, and a pseudo steady can be differentiated. However, the higher current density values reached during the coating synthesis on the mild steel reveal some structural differences. The coating thickness can be higher for the carbon steel, or the porosity reached can be different. The structure and the geometry of both layers are analysed in next section.
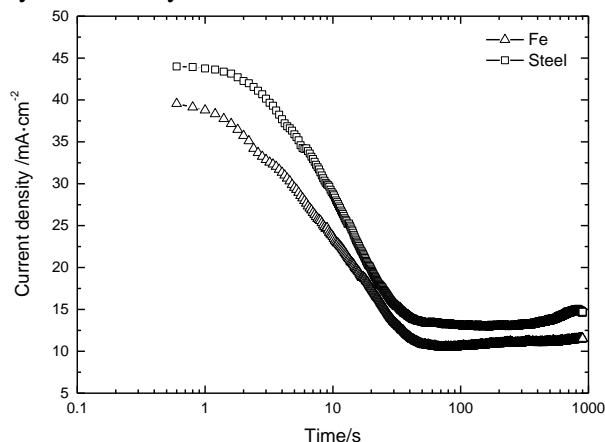

Fig. 1. Chronoamperograms obtained during the anodizing of carbon steel and Fe substrates in ethylene glycol containing water (3%) and 0.1M NH_4F.

Morphological characterization of the conversion coatings

The morphology of the formed FeF_3 layers was analysed by SEM. The general appearance clearly shows a difference between both coatings. The conversion coating generated on the iron is continuous (Fig. 2a) while the conversion coating synthesized on the mild steel strips reveals the grain boundaries (Fig. 2d), which is because of the reduced growth at grain boundaries.

The SEM images presented in Fig. 2 are arranged in increasing magnification (from left to right). The upper row (Fig. 2a-c) corresponds to the iron substrate and the lower row (Fig. 2d-f) to the steel substrate. A well-developed porous nano-structure can be observed for both substrates. The average pore diameter is similar in both samples; around 75 nm and the density of pores can be estimated at about 10^{10} pores cm^{-2}. Based on these parameters and assuming cylindrical geometry, the open porosity can be estimated at around 44% for both coatings.
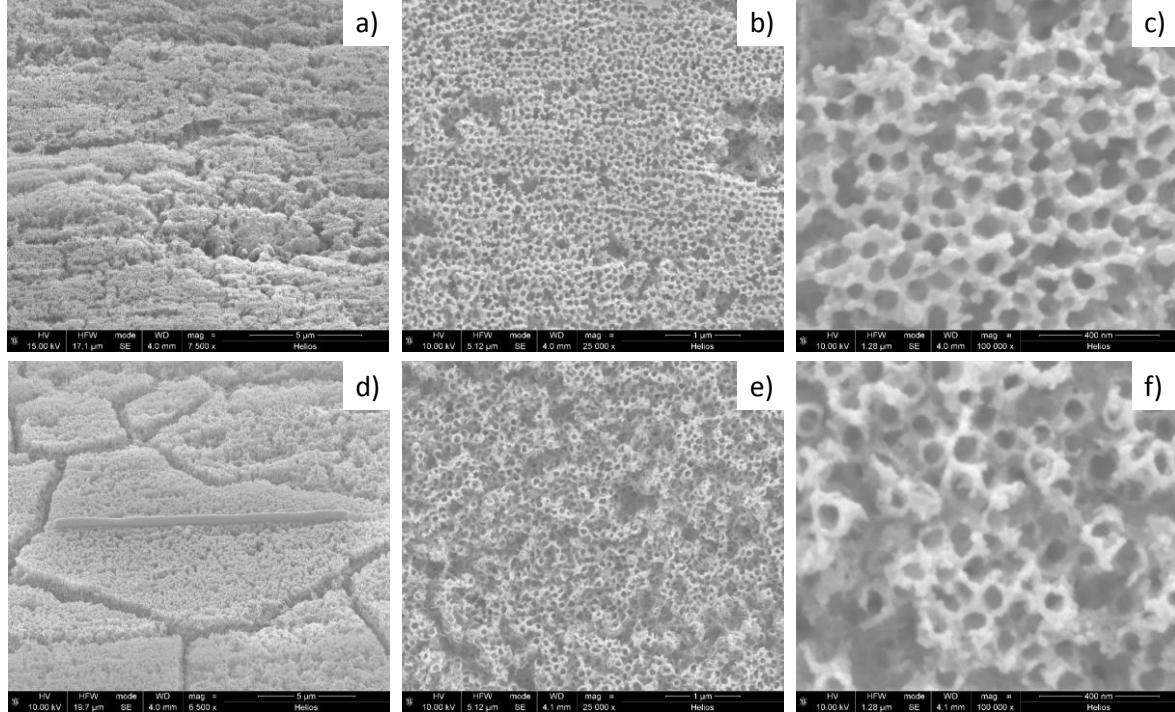

Fig. 2. SEM images of the FeF_3 conversion layers synthesized. The upper row corresponds to the iron substrate, and the lower row to the steel substrate. Magnification increases from left to right. a) 7500x; d) 6500x; b), e) 25000x; c), f) 100000x.
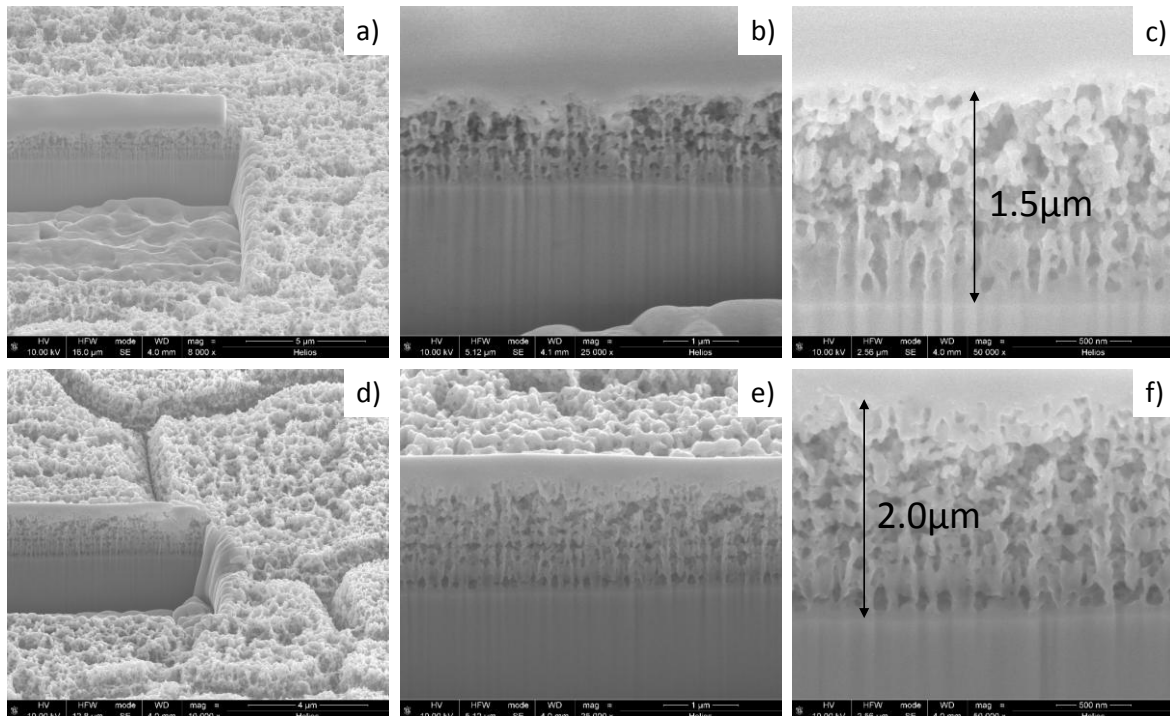

Fig. 3. FIB-SEM images of cross sections of the synthesized FeF_3 coatings. The upper row corresponds to the iron substrate, and the lower row to the steel substrate. (a and d) general view of the section created by Ga^+ bombardment. (b and e) detail of the layer cross sections with, on top, the Pt layer deposited for conductivity purposes. (c and f) detail of the layer's cross section showing the estimated thickness

Figure 3 summarizes the FIB-SEM observations aimed at obtaining information about the thickness and morphology of the coatings. Figures 3a and 3d clearly show the difference in grain boundaries specific to the steel substrate. The coating is thinner at those regions. The general view presented in Figures 3b and 3e shows that the coating is thinner for the iron substrate than for the steel substrate. The detailed view given in Figures 3c and 3f reveals that the FeF_3 layer generated on the iron strips is thinner than that generated on the mild steel. The layer for the iron substrate is about 1.5 µm thick, while on the mild steel this reaches 2.0 µm. This result is in concordance with the higher current density recorded during the anodizing process for the steel substrate.

The images of Figure 3 also show clearly a homogeneous high porosity from the top to the bottom of the layer that guarantees the access of the electrolyte to the substrate. Nevertheless, the geometry of the pores shown in Figures 3c and 3f deviate somehow from the cylindrical shape. The diameter of the pores bottom seems smaller than at the pores mouth. So, considering the pore geometry as conical instead of cylindrical, as considered according to Figure 2, the estimated porosity results three times lower, around 17% open porosity.

Using the thickness and porosity data, we were able to estimate the mass of active material per surface unit. The maximum active mass corresponds to the conical-shaped pores (i.e., 0.658 mg·cm^{-2}) for the FeF_3 coating on steel and 0.494 mg·cm^{-2} for the coating on iron. The minimum active mass corresponds to the cylindrical-shaped pores (i.e. 0.433 mg·cm^{-2}) for the FeF_3 coating on steel and 0.325 mg·cm^{-2} for the coating on iron.

The elemental composition of FeF_3 coatings synthesized on mild steel was analysed using the EDX capability of the SEM. The chemical composition is given in Table 2. The formation of FeF_3 is confirmed by the Fe/F ratio. Moreover, the enrichment in C with respect to the matrix is confirmed. Comparing Tables 1 and 2, the atomic ratio C/Fe increases by one order of magnitude. The presence of O corresponds to partial surface hydration of the fluoride layer, in the form of $FeF_x(OH)_y$.

Table 2. EDX analysis of the conversion coating synthesized on the mild steel substrate.

	C	Fe	F	O
Weight%	2.03	82.52	9.31	3.1
Atomic%	7.19	62.83	20.84	8.24

Electrochemical characterization

Model of behaviour

The Nyquist diagrams of both coatings obtained directly in fresh synthesis electrolyte are depicted in Fig. 4. Two main aspects are of interest in these plots. The high frequency shift observed in detail in the inset of Fig. 4, and the diffusion-like feature observed for frequencies lower than 1 Hz.

The presence of a high frequency shift with a nearly 45° slope, for nominally constant cell geometry and electrolyte properties, can only be understood assuming a potential distribution through the pores of the FeF_3 structure formed. The model proposed by Macdonald for porous magnetite-based layers on steel [8] can be applied here. The corresponding impedance function, Eq. 1, contains a purely resistive term, which is the parallel association of the solid and liquid phases resistivities (R_m and R_s, respectively) times the thickness of the coating, L. Thus, the high frequency limit of the impedance contains two terms, the (constant) electrolyte resistance plus the variable part corresponding to the layer conducting properties.

The low-frequency diffusional tail can be attributed to the relaxation of fluorides, in excess in the pore network upon anodizing, or to oxygen diffusion associated to the corresponding cathodic reaction at pore walls that continue to sustain the iron corrosion at pore bottom[9]. In fact, the diffusion layers of the individual pores will overlap to some extent leading to a nearly planar diffusion feature[10].

The impedance spectra in the frequency window from 100 kHz to 1 Hz provides information about the microstructure and reactivity of the conversion layer. The experimental data were modelled using Eq. 1, where R_0 corresponds to the electrolyte resistance between the reference electrode and the pores mouth. R_m represents the resistance per unit of length of the fluoride phase, and R_s corresponds to the resistance per unit of length of the electrolyte inside the pores. Z_2 represents the impedance at the bottom of the pores and Z_1 is the interfacial impedance at the wall of the pore. Both impedances contain a resistive term, R_i, corresponding to the charge transfer, in parallel to a capacitive term, C_i, that holds for the corresponding double layer capacitance. A Cole-Cole dispersion term, α_i, has also be considered for each R_iC_i time constant. Figure 5 corresponds to a representation of the equivalent circuit parameters associated with the morphology of the pore structure as seen in the SEM images discussed in the previous section.

$$Z(\omega) = R_0 + \frac{R_m \cdot R_s}{R_m + R_s} \cdot L +$$

$$\frac{\sqrt{\gamma}(2R_m R_s + (R_m^2 + R_s^2)\cosh(L\sqrt{\gamma})) + \delta R_s^2 \sinh(L\sqrt{\gamma})}{\sqrt{\gamma}(R_m + R_s)(\sqrt{\gamma}\sinh(L\sqrt{\gamma}) + \delta \cosh(L\sqrt{\gamma}))} \quad (1)$$

with

$$\gamma = \frac{R_m + R_s}{Z_1(\omega)}, \quad \delta = \frac{R_m + R_s}{Z_2(\omega)},$$

$$Z_i(\omega) = \frac{R_i}{1 + (j\omega R_i C_i)^{\alpha_i}} \quad (i = 1, 2)$$

The impedance data presented in Fig. 4 were modelled using the equivalent circuit given in Fig. 5. To match the experimental data with the physical model, only the frequency window relevant to the coating microstructure and reactivity was considered, (i.e. 100 kHz to 1 Hz).
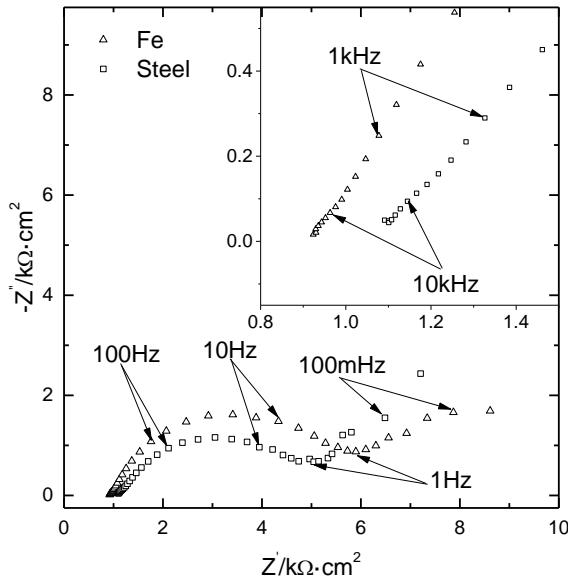

Fig. 4. Nyquist impedance diagrams obtained in fresh synthesis electrolyte after completing the anodizing process.

The fitted data reported in Table 3 clearly show the distinct electrical behaviour between the conversion layers formed on iron and mild steel. As it concerns the main objective of the study, the improvement of the fluoride solid phase conductivity, we can confirm that our hypothesis was good because the conductivity increases. The

R_m parameter value decreases by one order of magnitude, from 3.0 to 0.3 MΩ cm, probably due to the incorporation of C to the FeF_3 structure. The kinetic parameters, R_1 and R_2 are also lower for the coating developed on the steel substrate, which indicates faster reaction rates at both of the interfaces, the pore walls and pore bottom.
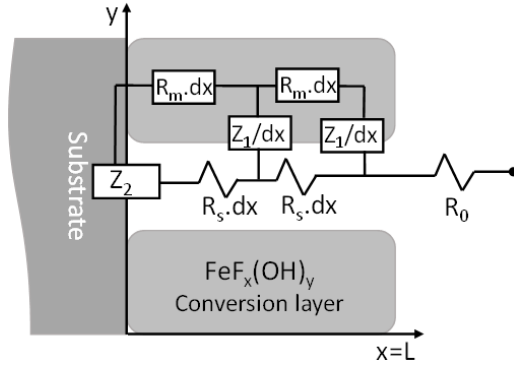

Fig. 5. Equivalent circuit corresponding to the synthesized iron fluorides porous structures. The impedance function is given in the Equation (1).
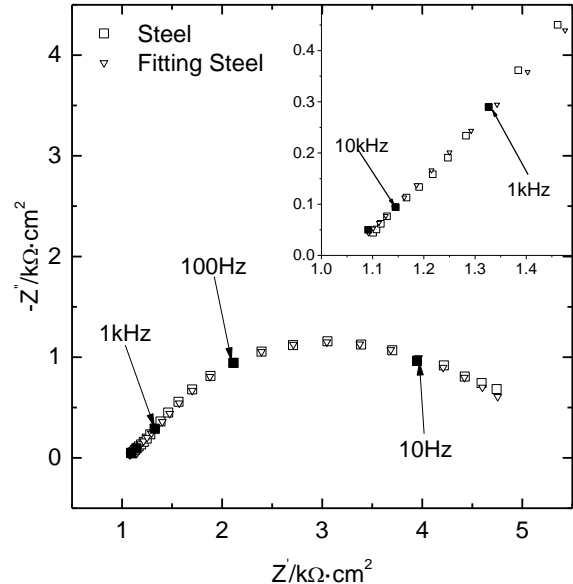

Fig. 6. Experimental and fitted impedance data corresponding to the steel sample in Fig. 6. The frequency window was limited to f> 1Hz. The impedance data were modelled using Eq. 1. The best fitting parameters are collected in Table 3.

Table 3. Best fitting parameters for the impedance data in Fig. 4 using Eq. 1 to model the impedance data. The frequency window was 100 kHz to 1 Hz. The coating thickness was fixed to 2 μm.

	R_0 $\Omega \cdot cm^2$	R_m $M\Omega \cdot cm$	R_s $M\Omega \cdot cm$	R_1 $M\Omega \cdot cm^3$	C_1 $mF \cdot cm^{-3}$	α_1	R_2 $k\Omega \cdot cm^2$	C_2 $\mu F \cdot cm^{-2}$	α_2	L μm
Fe	494	3.08	5.66	2.32	3.2	1	4.4	1.3	0.64	2
Mild Steel	988	0.31	10.0	1.85	8.3	1	2.6	6.0	0.50	2

Ageing of the conversion coating

In a recent investigation, the feasibility of obtaining in-situ active material by direct corrosion of Fe in the presence of an oxidizing electrolyte (LiPF$_6$) was demonstrated[11]. The objective here was to study the stability of the FeF$_3$ conversion layers formed on the steel substrate in the presence of a non-oxidizing Li salt, such as LiBOB. The impedance results, obtained in a symmetrical pouch cell at the null potential difference between both

electrodes, are presented in Fig. 7. A clear evolution is observed during the first 5 h of immersion, with the presence of a diffusional tail similar to that observed in Fig. 4. From 10 h onwards, the resistance associated to the time constant centred at about 1 Hz increases initially and remains unchanged after about 40 h, at which point the diffusion tail has completely moved outside of the considered frequency window. The high frequency part of the spectrum remains essentially unchanged after about 15 h.
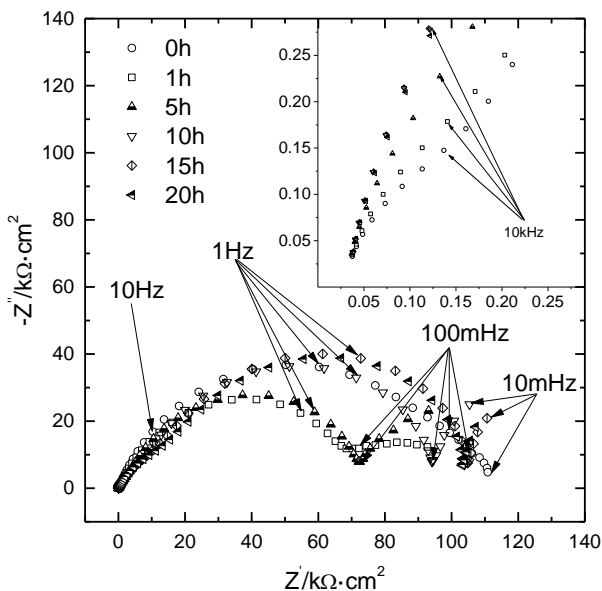

Fig. 7. EIS evolution of the conversion coating grown on mild steel and assembled in a symmetrical cell using 1 M LiBOB + 2% FEC in EC:DME (1:1 [v/v]).
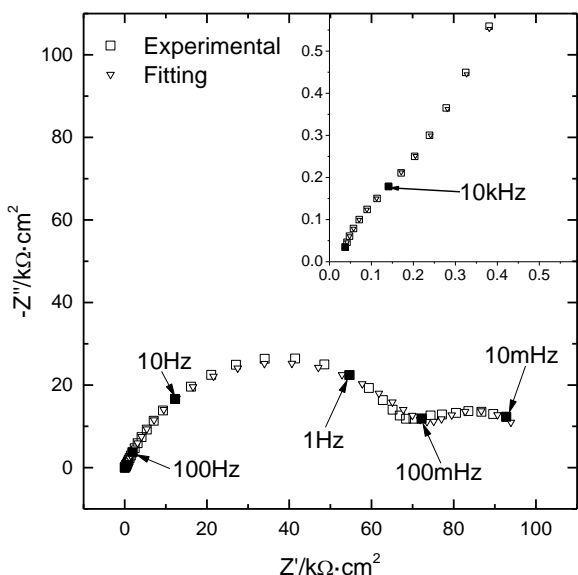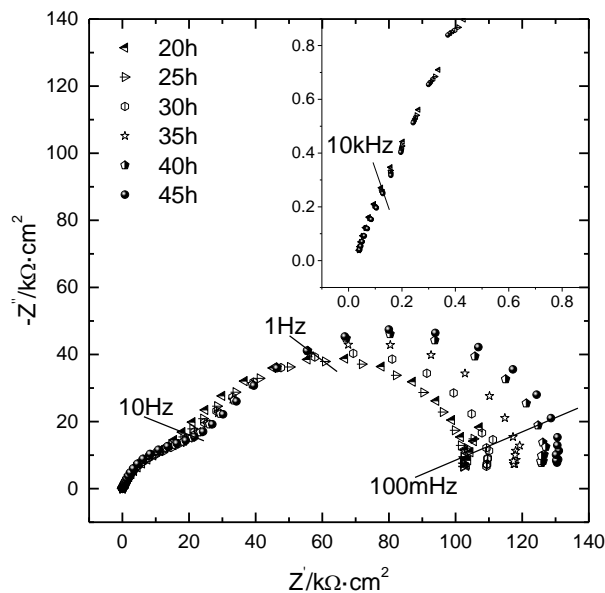

Fig. 8. Experimental impedance data obtained after 1h in the symmetrical cell and fitted data using Equations 1 and 2 as model impedance.

The interpretation of the impedance spectra presented in Fig. 7 is similar to that given in section

3.3.1, with the only difference being the cathodic reaction involved. As no oxidants are present in the electrolyte, one can imagine self-corrosion of Fe as Fe^{2+} at the pore bottom sustained by the reduction process Fe^{3+}/Fe^{2+} at the pore walls. The cathodic reaction will involve Li$^+$ insertion in the fluoride-based structure for electro-neutrality reasons. In parallel, BOB$^-$ will migrate to the pores bottom to compensate the Fe^{2+} charge being generated. Overall, a linear diffusion from the electrolyte can be considered, involving Li$^+$ and BOB species for the cathodic and anodic process, respectively.

Figure 8 corresponds to an example of the performance of the model described here. The pore structure of the layer is described by Eq. 1 and the linear diffusion, Z_d, (in series) by Eq. 2, where R_d corresponds to the diffusion resistance and τ_d to the diffusion time constant (δ^2/D). To describe the small high frequency arc observed in the inset of Fig. 8, it was necessary to include a 99 nF capacitance in parallel to the impedance of the coating, which accounts for the geometrical capacitance of the coating.

$$Z_d(\omega) = R_d \frac{tanh(\sqrt{j\omega\tau_d})}{(\sqrt{j\omega\tau_d})} \qquad (2)$$

The best fitting parameters for the selected times of evolution are summarised in Table 4. The evolution of R_1 shows an initially fast cathodic process, associated with Li^+ insertion, which slows down with immersion time. The Li^+ insertion (and Fe^{3+} reduction) leads to an increase of the coatings conductivity (R_m decreases with time, as the ratio Fe^{2+}/Fe^{3+} increases). The associated structural change leads to some pore blocking (R_m increases from 1 to 76 $M\Omega$ cm). Comparing the nearly constant R_2 values and the R_1 evolution, it is clear that the cathodic reaction represents the final energy barrier for stopping the self-transformation of the coating.

Cycling in a pouch cell

Charge and discharge curves of the conversion coating of FeF_3 developed on mild steel are shown in Fig. 9. A voltage plateau is observed around 1.8 V which is in agreement with a conversion reaction, according to the literature [12]. The specific capacity recorded during the first cycle corresponds to the theoretical value for FeF_3 (712 mA h g^{-1}) if a cylindrical porosity is considered (see section 3.2). If a conical geometry is considered, the specific capacity drops by 32%, to 483 mA h g^{-1}. The real value will lie between both limits.

During the second discharge the coating capacity values experience a noticeable decrease (43%), indicating that the process is not as reversible as expected. However, comparing this loss of capacity of the conversion coating on mild steel to that obtained on iron [3], the difference is only 7%, which can be considered a good result owing the difference in potential windows. The layer on iron was cycled between 4.0 V and 1.5 V while the coating on mild steel was cycled in the potential window 4.0 V to 1.0V, a deeper discharge that induces more irreversible changes in the active material.

Table 4. Fitting parameters obtained for the fitting data in Fig. 7 to the impedance given in Equation (1) and Equation 2.

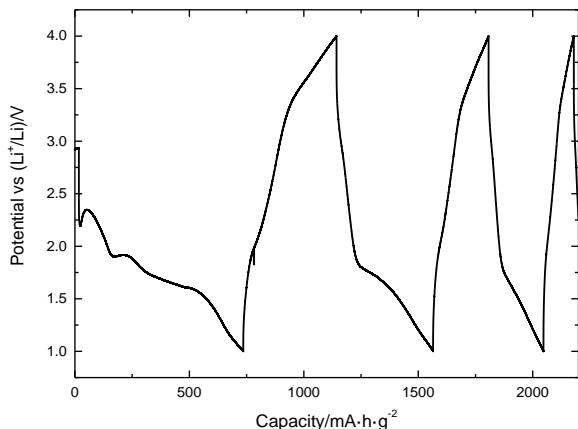|	R_0 $\Omega\cdot cm^2$	R_m $k\Omega\cdot cm$	R_s $M\Omega\cdot cm$	R_1 $M\Omega\cdot cm^3$	C_1 $mF\cdot cm^{-3}$	α_1	R_2 $k\Omega\cdot cm^2$	C_2 $\mu F\cdot cm^{-2}$	α_2	R_d $k\Omega\cdot cm^2$	T_d s	L μm
0h	14.6	371	1.05	0.04	183	0.74	51.5	0.120	0.91	5.1	9.98	2
1h	12.9	61.0	1.87	0.18	195	0.76	34.8	0.019	0.66	14.3	19.90	2
5h	16.3	278	5.50	2360	1.43	1	42.6	1.60	0.65	---	---	2
45h	23.0	3.6	75.8	36000	5.70	1	53.9	4.50	0.83	---	---	2

Fig. 9. Discharge and charge curves of a FeF_3 conversion layer grown on mild steel substrate. The electrolyte was 1 M LiBOB salt + 2% FEC in 1:1 EC: DMC. The charge density was calculated assuming cylindrical geometry for the pores (see text).

CONCLUSIONS

Based on our data, the following conclusions can be drawn:

a) FeF_3 conversion layers were developed on iron and mild steel substrates. The layers on steel substrates are thicker than on iron substrate.

b) EIS was successfully employed to study the microstructure and properties of the layers formed. The layers formed on mild steel are of higher conductivity than those formed on iron.

c) FeF_3 conversion layers immersed in LiBOB electrolyte tend to transform partially incorporating Li^+, as evidenced by the EIS results.

d) The FeF_3 conversion layers developed on mild steel substrate are able to cycle in Li-ion battery configuration with performance similar to that found for layers developed on pure iron.

REFERENCES

1. F. Badway, N. Pereira, F. Cosandey, G.G. Amatucci, Carbon-Metal Fluoride Nanocomposites, *J. Electrochem. Soc.* **150**, A1209 (2003).
2. F. Badway, F. Cosandey, N. Pereira, G.G. Amatucci, Carbon Metal Fluoride Nanocomposites, *J. Electrochem. Soc.* **150**, A1318 2003).
3. B. Guitián, S. Lascaud, X.R. Nóvoa, L. Ribeaucourt, E. Vidal, On the growth of nanostructured iron hydroxy-fluorides for Li-ion batteries, *J. Power Sources.* **241**, 567 (2013).
4. E. Vidal, L. Ribeaucourt, X.R. Nóvoa, B. Guitián, Metal halide electrode with improved conductivity, and associated production method, EU patent WO 2017102424, 2017.
5. C.C. Nguyen, B.L. Lucht, Comparative Study of Fluoroethylene Carbonate and Vinylene Carbonate for Silicon Anodes in Lithium Ion Batteries, J. *Electrochem. Soc.* **161**, A1933 (2014).
6. V. Aravindan, J. Gnanaraj, S. Madhavi, H.-K. Liu, Lithium-Ion Conducting Electrolyte Salts for Lithium Batteries, *Chem. - A Eur. J.* **17**, 14326 (2011).
7. S.S. Zhang, A review on electrolyte additives for lithium-ion batteries, *J. Power Sources.* **162**, 1379 (2006).
8. J.R. Park, D.D. Macdonald, Impedance studies of the growth of porous magnetite films on carbon steel in high temperature aqueous systems, *Corros. Sci.* **23**, 295 (1983).
9. B. Díaz, B. Guitián, X.R. Nóvoa, M.C. Pérez, The effect of long-term atmospheric aging and temperature in the electrochemical behaviour of steel rebars in mortar, *Corros. Sci.* **140**, 143 (2018).
10. N. Godino, X. Borrise, F.X. Muñoz, F.J. Del Campo, R.G. Compton, Mass transport to nanoelectrode arrays and limitations of the diffusion domain approach: theory and experiment, *J. Phys. Chem. C.* **113**, 11119 (2009).
11. E. Vidal, L. Ribeaucourt, X.R. Nóvoa, B. Guitián, Self-forming metal halide electrode, and associated production method, EU patent WO2017102427, 2017.
12. N. Pereira, F. Badway, M. Wartelsky, S. Gunn, G.G. Amatucci, Iron Oxyfluorides as High Capacity Cathode Materials for Lithium Batteries, *J. Electrochem. Soc.* **156**, A407 (2009).

ЕИС като инструмент за охарактеризиране на наноструктурирани слоеве железен флуорид за катодни материали в литиево-йонни батерии

Б. Гуитиан, Х.Р. Новоа, А. Пинтос*

Университет Виго, група ЕНКОМАТ, кампус Университетски, 36310 Виго, Испания

(Резюме)

В памет на проф. Здравко Стойнов за неговата невероятна личност и иновативен научен принос към електрохимията

Настоящото изследване има за цел да разработи FeF_3 слоеве нанесени върху евтини подложки от мека стомана за използване като катодни материали в литиево-йонни батерии. Покритията, отложени в електролит на базата на етилен гликол, се характеризират с помоща на SEM, FIB и EDX и показват образуването на аналогични порести структури, но с по- голяма дебелина на подложките от мека стомана, от колкото за железните подложки. Порестата структура се характеризира с ЕИС, използвайки линеен предавателен модел, който позволява да се определят значими параметри на слоя като проводимостта или реактивността на порите. Проводимостта на слоя от FeF_3 е по-висока за подложката от мека стомана, отколкото за подложката от желязо. Слоевете от FeF_3 до известна степен реагират в електролит от LiBOB, което се обяснява като корозия на желязото и редукция на Fe_3^+ с внедряване на Li^+ в структурата на FeF_3.